







In the format provided by the authors and unedited.

A map of the inorganic ternary metal nitrides

Wenhao Sun ^{1*}, Christopher J. Bartel², Elisabetta Arca³, Sage R. Bauers³, Bethany Matthews⁴, Bernardo Orvañanos⁵, Bor-Rong Chen⁶, Michael F. Toney ⁶, Laura T. Schelhas ⁶, William Tumas³, Janet Tate ⁴, Andriy Zakutayev³, Stephan Lany ³, Aaron M. Holder ^{2,3*} and Gerbrand Ceder^{1,7}

¹Materials Sciences Division, Lawrence Berkeley National Laboratory, Berkeley, CA, USA. ²Department of Chemical and Biological Engineering, University of Colorado, Boulder, CO, USA. ³National Renewable Energy Laboratory, Golden, CO, USA. ⁴Department of Physics, Oregon State University, Corvallis, OR, USA. ⁵Department of Materials Science and Engineering, Massachusetts Institute of Technology, Cambridge, MA, USA. ⁶SLAC National Accelerator Laboratory, Menlo Park, CA, USA. ⁷Department of Materials Science and Engineering, UC Berkeley, Berkeley, CA, USA. *e-mail: wenhaosun@lbl.gov; Aaron.Holder@colorado.edu

A Map of the Inorganic Ternary Metal Nitrides

Wenhao Sun^{1*}, Christopher J. Bartel², Elisabetta Arca³, Sage R. Bauers³, Bethany Matthews⁴, Bernardo Orvañanos⁵, Bor-Rong Chen,⁶ Michael F. Toney,⁶ Laura T. Schelhas,⁶ William Tumas³, Janet Tate,⁴ Andriy Zakutayev³, Stephan Lany³, Aaron M. Holder^{2,3*}, Gerbrand Ceder^{1,7}

¹ Materials Sciences Division, Lawrence Berkeley National Laboratory, Berkeley, California 94720, USA

² Department of Chemical and Biological Engineering, University of Colorado, Boulder, Colorado 80309, USA

³ National Renewable Energy Laboratory, Golden, Colorado 80401, USA

⁴ Department of Physics, Oregon State University, Corvallis, Oregon 97331, USA

⁵ Department of Materials Science and Engineering, Massachusetts Institute of Technology, Cambridge, MA 02139

⁶ SLAC National Accelerator Laboratory, Menlo Park, CA, 94025, USA.

⁷ Department of Materials Science and Engineering, UC Berkeley, Berkeley, California 94720, USA

*Corresponding Authors: wenhaosun@lbl.gov, Aaron.Holder@nrel.gov

Supplemental Information

Contents

1. Supplemental references for computational predictions of ternary nitrides
2. Construction and Clustering of Ternary Nitrides Map
 - a. Comparison of clustered nitrides map with a Pettifor nitrides map
3. Interactive Ternary Nitrides Map
4. Validation of Zn-Me-N and Mg-Me-N Predictions
 - a. Unconstrained Crystal Structure Prediction
 - b. Thin-Film Synthesis
 - c. Synchrotron Characterization
5. Nitride Discovery Histogram
6. Deepest Hull Binary Nitrides
7. Metallicity, Ionicity, and Covalency Calculations
8. Extended Metallicity/Ionicity/Covalency Figures
9. *Reductive Effect* stabilized structures - $\text{Co}_2\text{Mo}_3\text{N}$, $\text{Sr}_3\text{Ge}_2\text{N}_2$

S.I.1. Supplemental references for computational predictions of novel nitrides

Below, we provide some important examples of previous efforts to computationally predict novel binary and ternary nitride compounds and structures. This list serves to highlight a diversity of methods and nitride chemistries that have previously been explored computationally.

Aslam, Muhammad Aamir, and Z. J. Ding. "Prediction of Thermodynamically Stable Compounds of the Sc–N System under High Pressure." *ACS Omega* 3.9 (2018): 11477-11485.

Balasubramanian, Balamurugan, et al. "Magnetism of new metastable cobalt-nitride compounds." *Nanoscale* 10.27 (2018): 13011-13021.

Bannikov, V. V., I. R. Shein, and A. L. Ivanovskii. "Elastic properties of antiperovskite-type Ni-rich nitrides MNi_3 (M= Zn, Cd, Mg, Al, Ga, In, Sn, Sb, Pd, Cu, Ag and Pt) as predicted from first-principles calculations." *Physica B: Condensed Matter* 405.22 (2010): 4615-4619.

Bannikov, V. V., I. R. Shein, and A. L. Ivanovskii. "Structural, elastic and electronic properties of new antiperovskite-like ternary nitrides $AlNi_3$, $GaNi_3$ and $InNi_3$ as predicted from first principles." *Computational Materials Science* 49.3 (2010): 457-461.

Beznosikov, B. V. "Predicted nitrides with an antiperovskite structure." *Journal of Structural Chemistry* 44.5 (2003): 885-888.

Burghaus, Jens, et al. "Ternary nitride $GaFe_3N$: an experimental and quantum-theoretical study." *Inorganic chemistry* 49.21 (2010): 10148-10155.

Bykov, M., et al. "Fe-N system at high pressure reveals a compound featuring polymeric nitrogen chains." *Nature communications* 9.1 (2018): 2756.

Chen, Yi, Jiang Shen, and Nan-xian Chen. "The effect of Mo atoms in ternary nitrides with η -type structure." *Solid State Communications* 149.3-4 (2009): 121-125.

Dong, Jianjun, et al. "Theoretical study of the ternary spinel nitride system Si_3N_4 – Ge_3N_4 ." *Physical Review B* 67.9 (2003): 094104.

Gharavi, Mohammad Amin, et al. "Theoretical study of phase stability, crystal and electronic structure of $MeMgN_2$ (Me= Ti, Zr, Hf) compounds." *Journal of Materials Science* 53.6 (2018): 4294-4305.

He, Bing, et al. " $CuNi_3$: a new nitride superconductor with antiperovskite structure." *Superconductor Science and Technology* 26.12 (2013): 125015.

Huang, Bowen, and Gilles Frapper. "Barium–Nitrogen Phases Under Pressure: Emergence of Structural Diversity and Nitrogen-Rich Compounds." *Chemistry of Materials* 30.21 (2018): 7623-7636.

Huang, Jung Y., L. C. Tang, and M. H. Lee. "Ab initio study of the structural and optical properties of orthorhombic ternary nitride crystals." *Journal of Physics: Condensed Matter* 13.46 (2001): 10417.

Jaroenjittichai, Atchara Punya, and Walter RL Lambrecht. "Electronic band structure of Mg – IV – N_2 compounds in the quasiparticle-self-consistent $G W$ approximation." *Physical Review B* 94.12 (2016): 125201.

Jiang, Chao, Zhijun Lin, and Yusheng Zhao. "First principles prediction of vanadium and niobium nitrides with M_2N_3 stoichiometry." *Scripta Materialia* 63.5 (2010): 532-535.

Kroll, P., Schröter, T., Peters, M. Prediction of novel phases of tantalum (V) nitride and tungsten (VI) nitride that can be synthesized under high pressure and high temperature. *Angew. Chem., Int. Ed.* 2005, 44.27, 4249-4254.

Kroll, Peter, Bernhard Eck, and Richard Dronskowski. "First-Principles Studies of Extended Nitride Materials." *Advanced Materials* 12.4 (2000): 307-310.

Kvashnin, Alexander G., et al. "Computational search for novel hard chromium-based materials." *The journal of physical chemistry letters* 8.4 (2017): 755-764.

Lany, Stephan, et al. "Monte Carlo simulations of disorder in ZnSn N₂ and the effects on the electronic structure." *Physical Review Materials* 1.3 (2017): 035401.

Lyu, Sai, and Walter RL Lambrecht. "Quasiparticle self-consistent G W electronic band structure of Cd-IV-N₂ compounds." *Physical Review Materials* 1.2 (2017): 024606.

Niwa, Ken, Toshiki Terabe, Daiki Kato, Shin Takayama, Masahiko Kato, Kazuo Soda, and Masashi Hasegawa. "Highly Coordinated Iron and Cobalt Nitrides Synthesized at High Pressures and High Temperatures." *Inorganic chemistry* 56, no. 11 (2017): 6410-6418.

PalDey, S. C. D. S., and S. C. Deevi. "Single layer and multilayer wear resistant coatings of (Ti, Al) N: a review." *Materials Science and Engineering: A* 342.1-2 (2003): 58-79.

Papaconstantopoulos, D. A., and W. E. Pickett. "Ternary nitrides BiNCa₃ and PbNCa₃: Unusual ionic bonding in the antiperovskite structure." *Physical Review B* 45.8 (1992): 4008.

Punya, Atchara, and Walter RL Lambrecht. "CdGeN₂ and ZnGeO₅SnO₅N₂: Two new nitride semiconductors with band gaps in the blue-green." *Materials Science Forum*. Vol. 717. Trans Tech Publications, 2012.

Rached, D., et al. "Prediction study of the structural, elastic, electronic and optical properties of the antiperovskite BiNBa₃." *Solid State Communications* 149.45-46 (2009): 2002-2006.

Råsander, Mikael, and Michelle A. Moram. "Elastic constants of the II-IV nitride semiconductors MgSiN₂, MgGeN₂ and MgSnN₂." *Journal of Physics D: Applied Physics* 51.37 (2018): 375101.

Tholander, Christopher, et al. "Strong piezoelectric response in stable TiZnN₂, ZrZnN₂, and HfZnN₂ found by ab initio high-throughput approach." *Journal of Applied Physics* 120.22 (2016): 225102.

von Appen, Jörg, and Richard Dronskowski. "Predicting new ferromagnetic nitrides from electronic structure theory: IrFe₃N and RhFe₃N." *Angewandte Chemie International Edition* 44.8 (2005): 1205-1210.

Yu, Rongmei, et al. "Crystal structures of transition metal pernitrides predicted from first principles." *RSC Advances* 8.64 (2018): 36412-36421.

Yu, Shuyin, et al. "Exploring the real ground-state structures of molybdenum dinitride." *The Journal of Physical Chemistry C* 120.20 (2016): 11060-11067.

Yu, Shuyin, et al. "First-principles study of Zr-N crystalline phases: phase stability, electronic and mechanical properties." *RSC Advances* 7.8 (2017): 4697-4703.

Yu, Shuyin, et al. "Phase stability, chemical bonding and mechanical properties of titanium nitrides: a first-principles study." *Physical Chemistry Chemical Physics* 17.17 (2015): 11763-11769.

Zu, Lin, et al. "Observation of the Spin-Glass Behavior in Co-Based Antiperovskite Nitride GeNCo₃." *Inorganic chemistry* 55.18 (2016): 9346-9351.

S.I.2. Construction and Clustering of Ternary Nitrides Map

The stability information of a ternary chemical space can be represented on a heat map, constructed using axes corresponding to cations, and with a color scale corresponding to the formation energy of the lowest-energy compound in a ternary space. For a heat map with N elements on the axis, there are $N!$ (N factorial) possible cation orderings of the heat map axis. Simple ordering schemes can be chosen corresponding to atomic number, Mendeleev number, or another predefined elemental ordering derived from the Periodic Table. However, because these axes may not be ordered specifically with respect to underlying relationships within in a chemical space, stability trends and chemical families may not be readily apparent. For example, shown below is a heat map for the stable ternary nitrides, with elements on the axes ordered by atomic number:

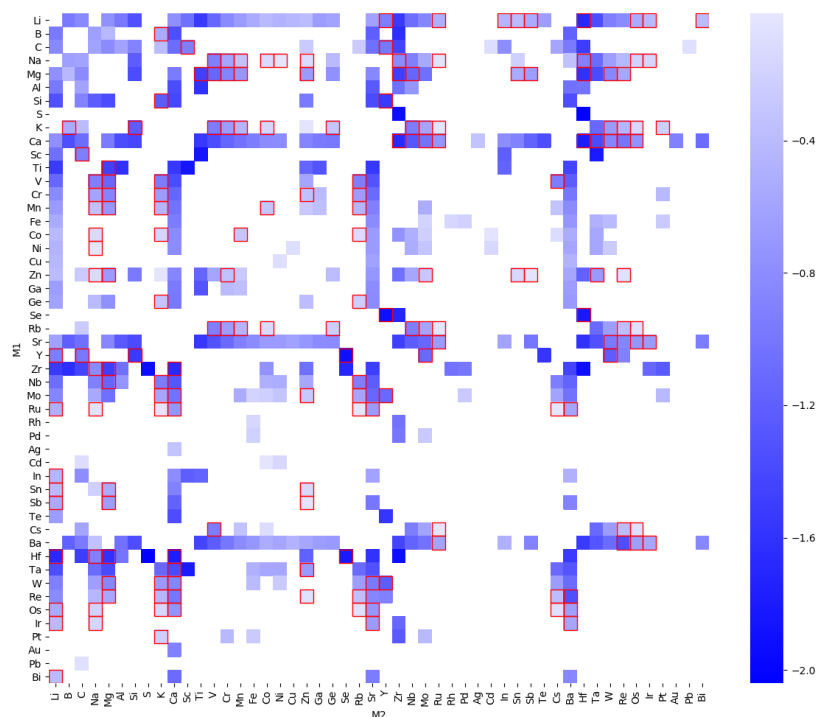


Figure S.I.2.1 Unclustered heatmap, where blue color scale corresponds to the formation energy of the ‘deepest-hull’ stable ternary nitride within a ternary M_1 - M_2 -N space.

Although some relationships between elements are apparent by identification, for example between Li, Ca, Sr, and Ba, other relationships are difficult to discern by eye. To construct a visualization that places ‘similar’ elements adjacent to one another, we use hierarchical agglomeration algorithms to cluster the ternary nitride space. Clustering requires a distance metric, represented by a vector for each element, A , indicating its ‘distance’ to all other elements, B . In available python packages, such as *scipy* or Seaborn, this distance is usually given by a single feature, for example, formation energy. Using this distance feature, a clustering algorithm iteratively determines which elements are ‘nearby’ other elements, gradually building larger and larger clusters. These clusters, and the distances between them, can be represented phenotypically by a dendrogram. Single-feature cluster maps are straightforward to construct, for example, using the *clustermap* function in the Seaborn package. Shown below are several single-feature clustermaps:

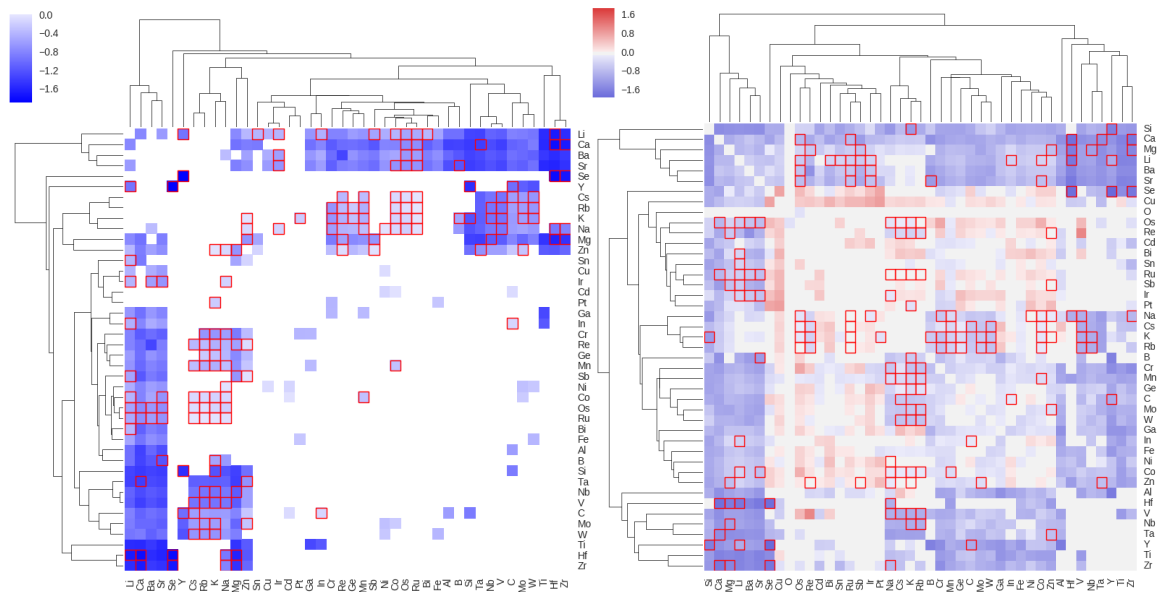


Figure S.I.2.2. Heatmaps clustered on the lowest formation-energy ternary nitride in a chemical space (*continuous data*) for **Left.)** stable ternary nitrides only, and **Right.)** including metastable ternaries.

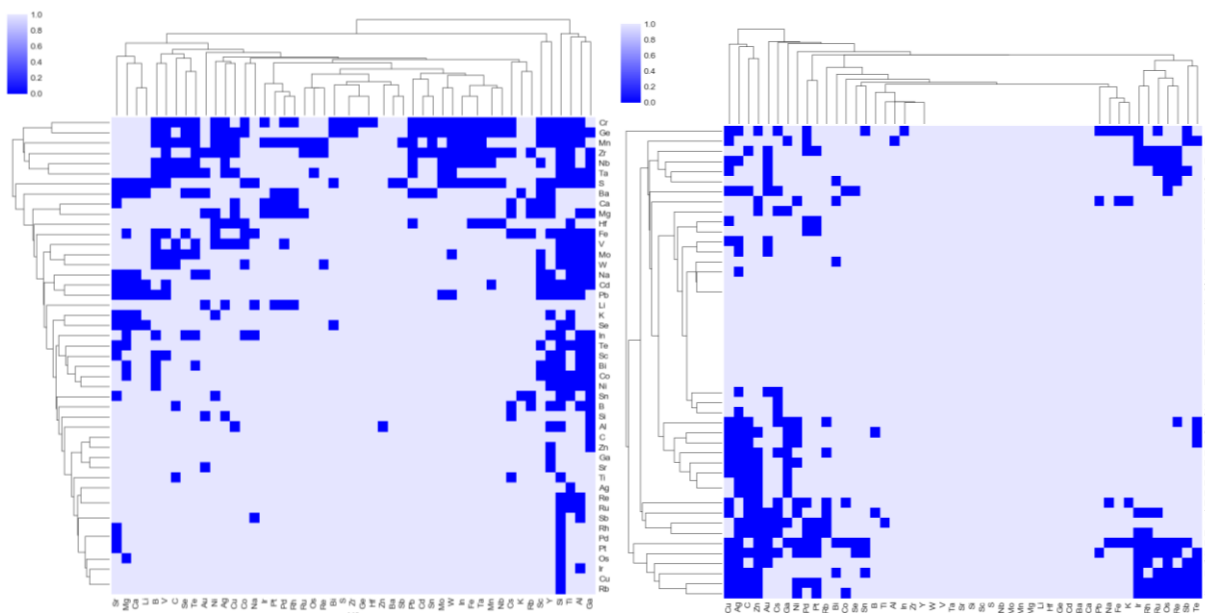


Figure S.I.2.3. Heatmaps clustered on nominal data, on whether the deepest compound in a ternary nitride space is **Left.)** metastable with respect to binaries (eventually on map as green), or **Right.)** metastable with respect to the elements (eventually on map as red).

For each singular feature, a dendrogram ordering and corresponding clustermap can be constructed. However, single-feature clustermaps present several limitations: 1) relationships constructed from different distance-metrics are difficult to cross-reference between maps, 2) dendrogram distances between elements with sparse features are not particularly meaningful, and 3) multiple relationships cannot be represented on the same figure.

To circumvent these limitations, we constructed a new multi-feature distance metric designed to capture multiple aspects of thermodynamic stability within the same figure. For the ternary nitrides map, our overarching objective is to elucidate which families of elements have similar thermodynamic propensity for forming ternary nitrides. At a high level, we aim to distinguish the elements by their propensity to form stable or metastable nitrides, and at a more local level, to group these elements by their formation energies and periodic groups. This data exists across multiple data types; formation energy is a continuous variable, periodic groups are ordinal, and the different types of stability (stable [blue], metastable against binaries [green], and metastable against elements [red]) are nominal.

To extend the single-feature clustermap algorithm to multiple data dimensions with mixed data-types, we used Gower’s metric.^{1,2} For each variable type, we choose a distance metric that is best suited to the data-type, and is scaled to fall between 0 and 1. For formation energy, which is continuous, we use the Euclidean distance. For the type of chemical family, which is an ordinal data type, we use the Manhattan distance on columns as defined in the left-step Periodic table,³ and for the stability-type, which is a nominal data type, we use the Dice metric.⁴ The Gower distance, G , is a linear combination of the various distance matrices,

$$G_{M_1-M_2} = \sum_i W_i \cdot d_{M_1-M_2}^i$$

Where W governs the weights of the various contributions. In our work, we emphasized the clustering features in the following priority: formation energy of the stable compounds, formation energy of all compounds, chemical families, and then proximity of similar ‘stability types’ (as indicated on the map as blue/green/red), as well as the white spaces (where the DMSP did not identify a reasonable compound substitution).

A custom implementation of Gower’s metric was coded within the *scipy* framework. Using the multi-feature distance matrix between the various elements, we calculate the linkages using the ‘average’ method (UPGMA algorithm) and construct a dendrogram with optimal leaf ordering.⁵ We manually re-arranged the leaves of the dendrogram so as to order the elemental axes from left to right predominantly by Stable (Blue) → Metastable vs. binaries (Green) → Metastable vs. elements (Red). The resulting 1-D ordering of elements is set as the axis for the multi-feature clustermap.

S.I.2.a Comparison of our clustered nitrides map with a Pettifor nitrides map

Below, in Figure S.I.2.a.1, we include a multicolored heatmap using a predetermined elemental orderings based Pettifor's Mendeleev numbers. There are some similarities between our hierarchically-clustered map and a map constructed using Pettifor's Mendeleev Numbers. For example, both maps capture many of the stable Alk-TM-N families.

However, there are several subtleties captured in our hierarchically-clustered ternary nitrides map, that are not apparent in a map constructed from Pettifor's Mendeleev numbers. For example:

- In the Pettifor map, the precious metals (Re, Ru, Os, Rh, Ir) are shuffled in between the first-row transition metals (Cr, Mn, Fe, Co, Ni), which results in the splitting of many clusters in the center of the map.
- Our clustered map places Mg next to Zn (rather than separated by Cd), and places these two elements with the rest of the Alkali/Alkaline Earths.
- In the Pettifor map, Sc and Y are not distinguished from the other transition metals, even though we found here that they do not react to form ternary nitrides with the same propensity as the other transition metals. This feature is captured by our hierarchical clustering, and was rationalized from the 'volcano plot' in Figure 3 of the manuscript.

One limitation of a ternary map constructed by a Mendeleev Number ordering is that there is no associated Dendrogram, which visualizes the distances between the different clusters. For example, while Cs and V are adjacent in the 1D-elemental ordering of our map, from the Dendrogram it is clear that Cs and V belong to different clusters. The same can be said between the boundaries at Al/Bi, Cu/Te, S/Sc, and even at a local level between the individual 'leaves' of the dendrogram tree. This clustering provides significant value in interpreting the chemical families in the ternary metal nitrides.

We note that it would not be straightforward to construct a Dendrogram for a predetermined ordering (such as the Mendeleev Numbers). This is because the Dendrogram is a product of the hierarchical clustering process, which ensures its smoothness and planarity (in other words, no criss-crossing branches or leaves). It is, in general, not possible to guarantee that a distance matrix visualized in graph form with arbitrarily set nodes (as in a predetermined elemental ordering) does not exhibit overlapping edges: see Kuratowski's theorem.

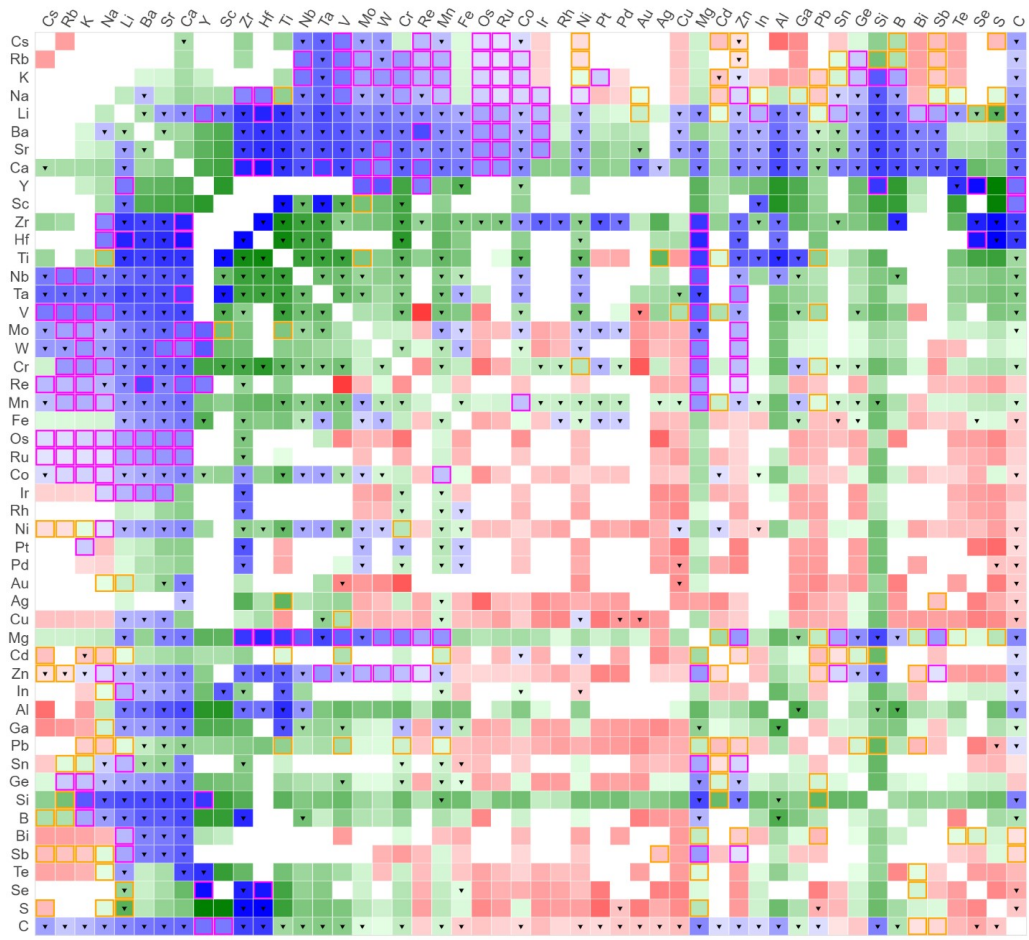


Figure S.I.2.a.1 Ternary Nitrides Map, as constructed using Pettifor’s Mendeleev numbers on the axes.

Using the methodology published in Reference S.6, we evaluate the ‘predictability’ of a ternary nitrides map, as ordered by the Mendeleev numbers, and by the hierarchical clustering performed in this work. To perform this assessment, we determine if the character of a single ‘box’ can be predicted by its neighboring boxes. We use the nearest-neighbor method from that paper to predict for each ternary M_1 - M_2 -N space if it should be stable (blue), metastable with $\Delta H_f < 0$ (green), or metastable with $\Delta H_f > 0$ (red).

The nearest-neighbor prediction works by determining the most common stability-type in the proximity of a sampled space. We evaluate the proximity by a radius determined by a usual Euclidean metric, so that for a space with coordinates (a, b) and (c, d) the distance r is given by $r = \sqrt{(c-a)^2 + (d-b)^2}$. For a given r , we count the most frequent stability-type in the neighboring spaces, these nearby spaces ‘vote’ on the character of a given box. A map that exhibits better clustering will have better prediction performance.

For this assessment, we will predict the color of the boxes of *new* ternary nitride spaces. However, we will only take into account the stability information from the *known* ternary nitrides (indicated on the original map by an inverted triangle). This way, both the Pettifor ordering and our ordering will be evaluated from equal footing (i.e., the state of the nitrides space before this work began). To illustrate how the nearest-neighbor prediction is performed: suppose we are predicting the stability of the Mg-Ti-N space, which was previously unknown, but was found to contain the stable $MgTiN_2$ phase during our DMSP/DFT investigation, and which subsequently synthesized in the laboratory (see manuscript Figure 2).

In Figure S.I.2.a.2 below, the Mg-Ti-N space is indicated by a yellow star. Using the nearest-neighbor assessment scheme, we can predict the color of the Mg-Ti-N space using our 1D ordering and Pettifor's 1D ordering. From our ordering, within a radius of $r = 1$, there are three blue boxes (and no red or green boxes), and so we would predict from our ordering that Mg-Ti-N is also blue (stable). In the Pettifor ordering, there are no known ternary nitride spaces (colored boxes) within $r = 1$ of Mg-Ti-N. However, if $r = 2$, there would be two blue boxes (and no red or green boxes), and so for the Pettifor ordering the nearest-neighbor assessment would also predict blue (stable), for $r = 2$.

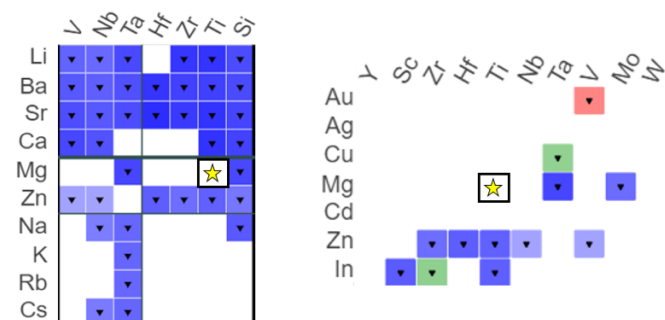


Figure S.I.2.a.2. Using the nearest-neighbor assessment to predict the stability-type (color) of the Mg-Ti-N space, using our ordering (Left) and the Pettifor ordering (Right).

We now evaluate our 1D elemental ordering and the Pettifor 1D ordering, using the nearest-neighbor assessment to predict each DMSP/DFT-surveyed space, using only the stability information of the *known* ternary nitride spaces. The results are shown below in Figure S.I.2.a.3.

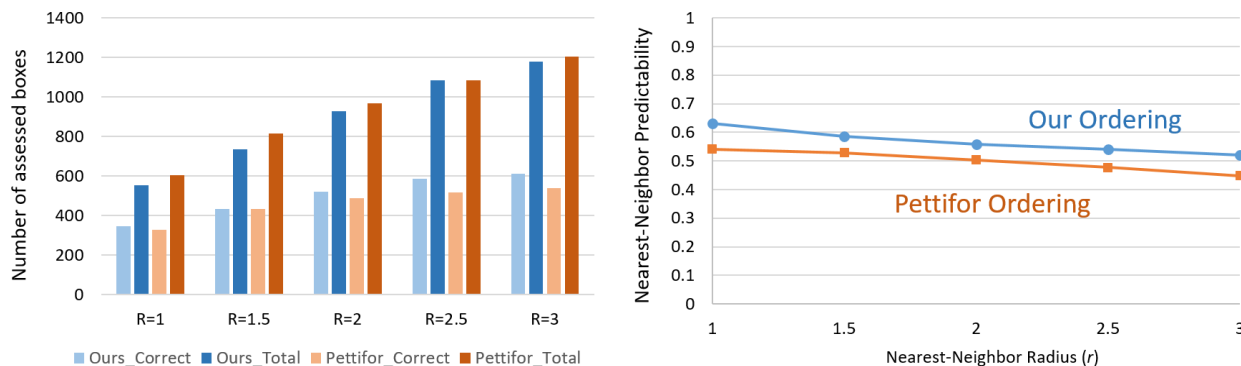


Figure S.I.2.a.3. Left) Bar charts showing the total number of correctly-predicted spaces vs. total surveyed spaces, using our 1D ordering (blue) and the Pettifor ordering (orange). **Right)** The accuracy of the nearest-neighbor prediction from a map constructed using our 1D elemental ordering, and the Pettifor 1D elemental ordering. When the search radius r is increased, prediction performance generally decreases, as we are sampling spaces that are further away, and therefore more isolated, from the known ternary nitrides.

Figure S.I.2.a.3. shows that for each DMSP/DFT space, our 1D ordering consistently predicts the stability-type of each space with higher accuracy than the Pettifor 1D ordering. This result is true for nearest-neighbor radii on the map ranging from $r = 1$ to $r = 3$. In other words, the chemical neighborhoods in our clustered ternary nitrides map are more predictive for the stability-type of a target ternary nitride space than in a Pettifor ordering.

S.I.3 Interactive map of ternary metal nitrides

To view the interactive ternary nitrides map, extract the attached **InteractiveTernaryNitridesMap.zip** file into a folder, and open **TernaryNitridesMap.html**. Hovering the mouse cursor over an individual M_1 - M_2 -N entry on the ternary nitrides map will show the corresponding ternary nitride phase diagram, along with a table of stable and metastable entries. An example is shown below for the Zn-Ti-N system.

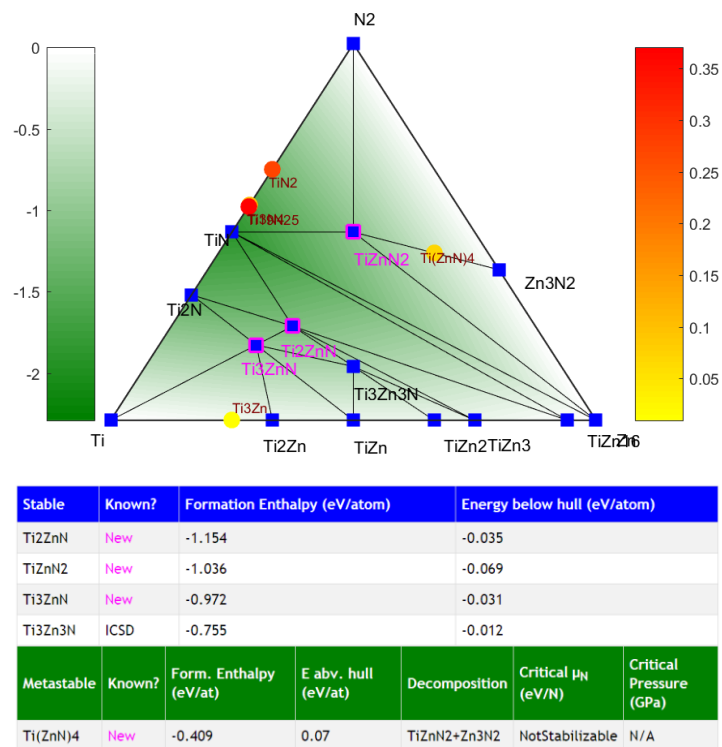


Figure S.I.3.1. Example ternary nitride phase diagram and table from the interactive map.

The green background of the ternary phase diagram corresponds to the depth of the ternary convex hull as a function of composition; color coded by the formation energy as shown on the left colorbar (units of eV/atom). Stable phases are indicated on the ternary phase diagram by a blue square. New stable ternaries predicted in this work are indicated by a magenta box (in this example, Ti₃ZnN, Ti₂ZnN, TiZnN₂). Stable ternaries without a magenta box (such as Ti₃Zn₃N) can be found in the ICSD. The ‘energy below hull’ indicates the reaction energy of a stable ternary nitride from its stable neighboring compositions in phase space.

Metastable compounds are indicated by a circle, with the energy above the hull indicated by the color bar on the right, in units of eV/atom. To avoid clutter, we only include metastable compounds with an energy above the hull < 400 meV/atom. Note that we previously found the 90th percentile of nitride metastability to be 200 meV/atom.⁷ If there are no ternary nitrides within 400 meV/atom of the hull, then the lowest formation energy metastable ternary is listed on the table. The table also includes the decomposition products of a metastable ternary nitride. For metastable ternary nitrides that decompose to N₂, we also provide a critical μ_N that can stabilize these metastable compounds, see Ref 8 for thermodynamic details. If a metastable ternary nitride can be stabilized under pressure, we also provide the transition pressure where it becomes stabilized.

The most up-to-date crystal structures for these compounds, along with their computed properties, can be obtained by searching for these compositions on the Materials Project.

The interactive map was programmed in Bokeh, an interactive python visualization library.⁹ Buttons on the bottom of the map can be used to turn on/off the ICSD triangles, the hover feature for phase diagram information, and the crosshair feature. Zooming in or out of the map using your internet browser (Ctrl + ‘=’/‘-’) may facilitate your viewing of the map. We recommend using the Google Chrome browser.

Running the interactive features of the map via the Bokeh interface may require an internet connection.

S.I.4 Validation of Zn-Me-N and Mg-Me-N Predictions

S.I.4.a. Unconstrained Crystal Structure Prediction

For the Zn-Mo-N, Zn-W-N, Zn-Sb-N, Mg-Ti-N, Mg-Zr-N, Mg-Hf-N, Mg-Nb-N systems, an unconstrained ground-state search was performed using the “Kinetically Limited Minimization” approach,¹⁰ which does not require prototypical structures from databases. Seed structures are generated from random lattice vectors and atomic positions, subject to geometric constraints to avoid extreme cell shapes, and to observe minimal interatomic distances (2.8 Å for cation-cation and anion-anion pairs, 1.9 Å for cation-anion pairs). For each material, we sampled at least 100 seeds, over the ternary compositions $A_iB_jN_k$ for $ijk = 112, 146, 414, 213, 124, 326, 338, 313$, chosen to accommodate the $(\text{Mg}/\text{Zn})^{2+}$, $M^{4+/5+/6+}$, and N^{3-} oxidation states. New trial structures are generated by the random displacement of one atom between 1.0 and 5.0 Å while maintaining the minimal distances. Trial structures are accepted if the total energy is lowered, and the number of trials equals the number of atoms in the unit cell.

S.I.4.b. Thin-Film Synthesis

Experimental synthesis of Zn-Me-N and Mg-Me-N thin-film sample libraries was carried out by combinatorial RF magnetron sputtering using high purity metals targets as cations sources. Ar and N_2 gas or Ar and activated N_2 by means of a nitrogen plasma source were used as sputtering gases. Two sputtering guns were loaded with 2"-diameter metal targets and positioned at 45° with respect to the substrate normal to achieve a cation compositional gradient; the N source was aligned to the normal. Prior to deposition, the sputtering chambers were evacuated to a pressure lower than 3×10^{-6} Torr. Eagle-XG glass or fused silica slides were used as substrates, chosen specifically to avoid any crystalline substrate effects which could stabilize metastable phases via coherent epitaxial strains. Before the deposition, the substrates were cleaned by degreasing in water and soap, followed by ultrasonic cleaning in acetone and isopropanol baths. Depositions were performed at a variety of pressure, gas flows, temperature, sputtering powers on the guns to achieve the desired crystalline phases. The deposition conditions used for the samples reported in this contribution are summarized below on Table S.I.4.1

We note that the ternary nitrides synthesized here are not simple solid-solutions of the binary nitrides, as the transition metal nitrides crystallize formally in the 3+ oxidation state (MoN, WN, SbN, TiN, ZrN, HfN, NbN), while Mg_3N_2 and Zn_3N_2 have Mg/Zn in the 2+ state. Therefore the transition metals oxidize (from 3+ \rightarrow 4+/5+/6+) in these ternary nitrides, indicating these are not alloys between the Mg/Zn-N binaries and the TM-N binaries. Finally, the energy scale of cation disordering was separately calculated to be < 10 meV/atom,¹¹ while these synthesized Zn-/Mg-ternary nitrides are stable by significantly more than 10 meV/atom. This indicates that the stability of these compounds is not driven by configurational entropy, and that these are indeed ground-state ternary compounds at these compositions.

Table S.I.4.1. Deposition conditions for reactive sputtering of Zn-Me-N and Mg-Me-N thin films.

	Mg-Ti-N	Mg-Zr-N	Mg-Hf-N	Mg-Nb-N
Dep. Temp	500 °C			
Substrate	EXG	EXG	EXG	f-SiO ₂
N₂ flow	6 sccm	6 sccm	6 sccm	6 sccm
Ar flow	6 sccm	6 sccm	6 sccm	6 sccm
Deposition pressure	3.5 mT	3.5 mT	3.5 mT	3.5mT
Mg power	40 W	40 W	30 W	40 W
TM power	60 W	60 W	50 W	40 W
N₂ power	350 W	350 W	300 W	350 W
Dep time	90 mins (150-300nm thick depending on composition)			
	Zn-Mo-N	Zn-W-N	Zn-Sb-N	
Dep. Temp	200	RT	300	
Substrate	EXG	EXG	EXG	
N₂ flow	10 sccm	10 sccm	10 sccm	
Ar flow	10 sccm	10 sccm	10 sccm	
Deposition pressure	20 mT	20 mT	20 mT	
Zn power	30	35 W	50	
M power	40 W	35 W	20 W	
N₂ power	250 W	-	-	
Dep time	60 mins (100-500nm thick depending on composition)			

S.I.4.c. Synchrotron Characterization

Spatially resolved characterization of the thin-film sample libraries was performed on a 4×11 grid consisting of 4 rows and 11 columns, with the compositional gradient along the 11 positions in one row. Cation composition was determined by quantitative XRF on Fischer Scientific instruments (Fischerscope XDV-SDD or Fischerscope XUV-XRF). Stylus profilometry (Dektak 8) or calibrated XRF were used to determine sample thickness. Data analysis was performed using custom-written procedures in the Wavemetrics IGOR Pro software package. The resulting data are available at htem.nrel.gov. Based on the results of the compositional analysis, sample points having the exact cation stoichiometry as to the theoretically predicted compounds, were subjected to high resolution x-ray diffraction measurements.

Wide-angle X-ray scattering (WAXS) was performed using the Stanford Synchrotron Radiation Lightsource (SSRL) Beamline 11–3 with an X-ray wavelength of 0.9744 Å. Two-dimensional scattering data were collected using a Rayonex MX225 detector in a grazing incidence geometry with the X-ray beam held at an incident angle of 3° and a sample to detector distance of 150 mm. Images are calibrated using a LaB6 standard and integrated between 10° < χ < 170° (χ is the polar angle) using GSAS-II.¹² Diffraction data presented in the main text were background subtracted using an ad-hoc Chebyshev function. Raw integrated line scans are shown in **Fig. S.I.4.c.1**. The broad signals at ca. 1.8 and 5 Å⁻¹ is from the amorphous substrates.

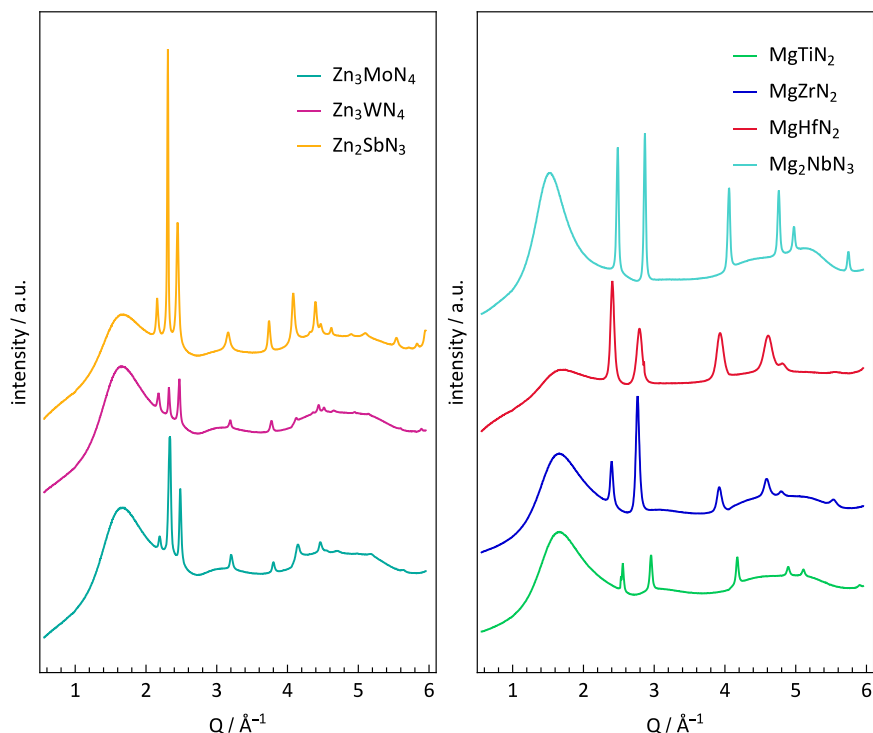


Figure S.I.4.c.1 Unprocessed line-scans generated from integrated detector images for (left) hexagonal Zn-containing compounds and (right) cubic Mg-containing compounds. Q relates to diffraction angle (θ) and incident wavelength (λ) by $Q = (4\pi/\lambda)\sin(\theta)$ and $\lambda = 0.9744$ Å

S.I.5 Ternary Nitride Discovery Histogram

Listed below are the years that each ternary M_1 - M_2 -N nitride space was discovered, as determined by the date of the publication for the first ternary nitride in that M_1 - M_2 -N system, as listed on the Inorganic Crystal Structure Database, shown in Figure 2d. Systems with stars are computed in DFT to be metastable (above the convex hull), corresponding to green or red squares in the ternary nitrides map.

1927 : C-Ca C-Ti*

1935 : Al-C

1938 : C-Na

1940 : C-K

1941 : C-Zn

1942 : C-Fe* C-Li

1945 : Au-C* C-Cd

1946 : Li-Mg Li-Zn

1948 : Ga-Li Al-Li

1949 : Li-Ni Cu-Li Co-Li

1950 : Nb-Ti* Ti-Zr* Nb-Zr* Nb-V* Ti-V*

1953 : Ge-Li Li-Si Li-Ti

1954 : Co-Mo Ni-Ti* Ni-Ta* Mo-Ni Co-Ti* Co-Ta* Mn-Ta* Ta-V* Fe-Ta*

1955 : Fe-Ni* Fe-Pt

1959 : Mn-Ni* Cr-Mn* Li-Mn Li-V Fe-Mn*

1960 : Hf-V* Hf-Zr* Hf-Ti* Hf-Ta* B-Zr* Fe-Pd

1961 : Cr-Li

1962 : Mn-Sn* In-Mn*

1963 : Al-Ti*

1964 : Hf-Zn Ag-Mn* Ti-Zn Nb-Zn Zn-Zr Ga-Ti In-Ti In-Zr* V-Zn Cr-Ga Ga-V* Al-Nb*
 Cu-Mn*

1965 : Au-V*

1966 : Re-Sr Pd-S*

1967 : Ni-Zr* Fe-Nb* Co-Zr* Cr-Ta* Re-Zr* Os-Zr* Mn-Nb* Cr-Nb* Co-V* Ir-Zr* Ni-V* Ru-Zr*
 Pd-Zr* Co-Nb* Fe-Zr* Hf-Nb* Nb-Ni* Rh-Zr* Pt-Zr* V-Zr*

1968 : Ge-Mn* Ga-Mn Fe-Ge*

1969 : Cr-Ge* Mn-Rh*

1970 : Ge-Mg Mg-Si Hf-Ni*

1971 : Mn-Pt* B-Ti* Cr-Ti* Mn-Si* Cr-Hf* Ge-V* Ge-Zn Mn-Zn Ca-Ge Li-Zr Cr-Zr*

1972 : Cr-Pd* Cr-Pt Mn-Pd* Cr-Sn* Cr-Rh* Ir-Mn* Cr-Ir*

1973 :

1974 : Nb-Ta* Ca-Ga

1975 : Cr-V* Ta-Ti* K-Zn Cs-Zn* Ta-Zr*

1977 : Sc-Ti* Mn-Ti* Cr-Sc* Sc-V* Mn-V*

1978 : Mo-Ta*

1979 : Mo-Nb*

1980 : Cd-K*

1981 : Cs-Sr*

1982 : Ba-Cs*

1983 : Rb-Zn*

1984 : Ca-Cs* Pb-S* Al-Hf* Ge-Na

1986 : B-Li Al-Zr*

1987 : In-Sr Ca-In

1988 : Sc-Ta* Co-Cs B-Nb*
 1989 : Ca-Li Na-Ta Cs-Ta K-Ta Rb-Ta Li-Sr Nb-Sc*
 1990 : Ca-Zn Ca-Cr B-Na Fe-Li Li-Mo Li-W Fe-Y* Ca-Fe Fe-Mo* Ca-Ni Ba-Ni
 1991 : Ba-W Cu-Ta* Ga-Nb* Ba-Fe Li-Ta Ba-Mo B-Mg* Cu-Pd*
 1992 : Na-W Sn-Zr* Li-Nb Bi-Ca Na-Nb Mo-Na Ca-Sb Fe-Sr Ca-Pb* Ca-V Ca-Sn Mg-Ta
 Ba-Na
 1993 : Na-Si Mn-Sr Ca-Mn Ba-Mn Co-Y* Au-Ca Ba-Ta Cs-Nb
 1994 : B-Sr Ba-Co Al-Sr Ba-Zr Ag-Ca B-Ca Fe-W Ba-Nb
 1995 : Sr-Zn Ba-V Ca-Mg Ba-Cr Ni-Sr Ba-Si Sr-V Ba-Zn Ba-Ti Ba-Ga Ga-Sr Ca-Si
 Si-Sr Mn-W*
 1996 : Sr-Zr Hf-Sr Ge-Sr Ba-Ge Cr-Sr Mn-Mo*
 1997 : Cr-W* Cu-Sr
 1998 : Ba-Hf Ba-Cu Sr-Ti Co-W* Nb-Sr Si-Zn Co-Sr Ni-W
 1999 : Al-Ba Al-Ca
 2000 : Na-Re Cs-Mn Rb-W Mo-Sr Cs-W Li-Re Cs-Mo
 2001 : Mo-Pd* Mg-Sr
 2002 : Au-Sr* Ba-Sr*
 2003 : Sr-Ta In-Sc* S-Zr Li-Sc B-Ba
 2004 : Ba-In Mo-Pt* Sb-Sr Ba-Bi Bi-Sr Ba-Sb
 2005 : Na-Sn* Ba-Pb* Pb-Sr* Fe-Rh Ba-Sn* Sn-Sr*
 2006 : Au-Cs* Ba-Li* Li-S* Au-Rb* Au-K* Ba-Rb*
 2007 : Ca-Ti Al-B* Ca-Co Ca-Nb Sc-Zr*
 2009 : Co-In* In-Ni* Fe-Ga*
 2010 : Cs-Pd* Al-Ga* Li-Te* Li-Se*
 2011 : Cd-Co Cd-Ni
 2012 : Se-Zr Mg-Mo Al-Si*
 2013 : Hf-S* Cu-Ni Ga-Mg*
 2014 : Te-Y Fe-Se* Au-Cu*
 2015 : Fe-Sn*

This Work Synthesized:

Mg-Hf, Mg-Ti, Mg-Zr, Mg-Nb, Zn-W, Mo-Zn, Sb-Zn

This Work Predicted (Stable Only):

Ir-Ba, Os-Ba, Re-Ba, Ru-Ba, Ru-Ca, K-Co, Na-Co, Co-Rb, Cr-K, Cr-Mg, Cr-Na, Cr-Rb, Cr-Zn, Y-C, Ge-
 K, Ge-Rb, Ca-Hf, Hf-Li, Na-Hf, Hf-Se, Li-In, Sr-Ir, K-B, K-Os, K-Pt, Re-K, Ru-K, K-Si, Bi-Li, Ir-Li, Os-
 Li, Ru-Li, Sb-Li, Y-Li, Mg-Zn, Mn-Co, K-Mn, Mg-Mn, Na-Mn, Mn-Rb, Mo-Ca, Mo-K, Mo-Rb, Y-Mo,
 Na-Ir, Na-Ni, Na-Os, Na-Ru, Na-Zn, Nb-K, Nb-Rb, Ca-Os, Cs-Os, Os-Rb, Sr-Os, Re-Ca, Cs-Re, Re-Mg,
 Re-Rb, Re-Zn, Cs-Ru, Ru-Rb, Ru-Sr, Sb-Mg, , Sc-C, Y-Se, Y-Si, Sn-Li, Mg-Sn, Zn-Sn, Ca-Ta, Zn-Ta, Cs-
 V, K-V, Mg-V, Na-V, Rb-V, Ca-W, K-W, Mg-W, Sr-W, Y-W, Ca-Zr, Na-Zr, Zn-Ni

S.I.6 Deepest Hull Binary Nitrides

Formation energy of the ‘deepest-hull’ binary nitride, as computed in DFT-PBE and using reference data from the MaterialsProject database. In systems where a binary nitride is unknown (for example, Au-N), the deepest-hull formation energy is computed from a binary nitride structure generated using the same DMSP employed in this work, computed previously by the authors in Reference 8.

*We note that in the Sr-N and Ba-N spaces, the deepest-hull binaries are actually SrN_2 ($\Delta H_f = -0.751$ eV/at) and BaN_2 ($\Delta H_f = -0.765$ eV/at). However, these compounds are diazenides,¹³ which result in electronic structures that we anticipate to be poor reference states for the solid-state bonding analyses. For this reason, we use Sr_3N_2 and Ba_3N_2 as the reference binaries for the Sr-N and Ba-N systems, which are constructed in DFT based on the Ca_3N_2 structure. We note that these Sr_3N_2 and Ba_3N_2 compounds have comparable formation enthalpies with SrN_2 and BaN_2 , as shown on the table below.

Convex hulls for the binary nitride spaces can be viewed for free on the Materials Project website, using the ‘Phase Diagram’ app.

Element	ΔH_f (eV/atom)	Compound	Element	ΔH_f (eV/atom)	Compound
Ag	0.57	Ag_3N	Nb	-1.21	NbN
Al	-1.59	AlN	Ni	-0.06	Ni_3N
Au	0.79	AuN	Os	0.05	OsN_2
B	-1.47	BN	Pb	0.33	Pb_3N_2
Ba	-0.76	* Ba_3N_2	Pd	0.23	PdN_2
Bi	0.24	BiN	Pt	0.19	PtN_2
C	0.14	C_3N_4	Rb	0.48	Rb_3N
Ca	-0.95	Ca_3N_2	Re	-0.13	Re_3N
Cd	0.39	Cd_3N_2	Rh	0.11	RhN_2
Co	-0.08	CoN	Ru	0.11	RuN_2
Cr	-0.53	CrN	S	0.35	SN
Cs	0.35	Cs_3N	Sb	0.18	SbN
Cu	0.19	Cu_3N	Sc	-2.11	ScN
Fe	-0.31	FeN	Se	0.63	SeN
Ga	-0.67	GaN	Si	-1.31	Si_3N_4
Ge	-0.26	Ge_3N_4	Sn	0.00	Sn_3N_4
Hf	-1.94	HfN	Sr	-0.75	* Sr_3N_2
In	-0.11	InN	Ta	-1.37	TaN
Ir	0.16	IrN_2	Te	0.68	Te_3N_4
K	0.38	K_3N	Ti	-1.91	TiN
Li	-0.46	Li_3N	V	-1.16	VN
Mg	-0.91	Mg_3N_2	W	-0.46	WN
Mn	-0.41	MnN	Y	-1.88	YN
Mo	-0.55	MoN	Zn	-0.03	Zn_3N_2
Na	0.26	Na_3N	Zr	-1.87	ZrN

S.I.7 Metallicity, Ionicity, and Covalency Calculations

The Density Derived Electrostatic and Chemical (DDEC) approach was used to obtain net atomic charges and natural bond orders assigned to each ion in each calculated structure.^{14,15} From the DDEC analysis we define the average charge for ion i , δ_i , as the net atomic charge assigned to ion, i (number of electrons) averaged over all ions, i , in the structure, $A_\alpha B_\beta N_\gamma$. The summed bond order for ion i , s_i , was obtained similarly by summing the natural bond orders for all interactions containing i , averaged over all ions, i , in the structure, $A_\alpha B_\beta N_\gamma$. The Crystal Orbital Hamilton Population (COHP) analysis was used to quantify the bonding interactions within each structure and partition these interactions by specific ion-ion pairs using the LOBSTER code.¹⁶ To normalize the comparison of COHPs across a range of structures and compositions, the energy levels from each PBE calculation were aligned to core levels. Doing so allows for a reasonable comparison of Fermi energies and thus COHP energy depths across the various systems analyzed. To alleviate the effects of varied pseudopotentials across systems, the number of free atom valence electrons was determined for each system using the following equation:

$$N_v(A_\alpha B_\beta N_\gamma) = \alpha N_v(A) + \beta N_v(B) + \gamma N_v(N)$$

where N_v is the number of valence (outermost shell) electrons. The minimum energy which contains valence electrons, ε_V was then determined for each structure by incrementally decreasing the energy, ε , and integrating the density of states (DOS) from ε to the Fermi energy, ε_F , such that

$$\varepsilon_V = \varepsilon_V: \int_{\varepsilon_V}^{\varepsilon_F} DOS(E') dE' = 1$$

where DOS is normalized by N_v and E' is the core-level aligned energy. The magnitude of bonding interactions, Σ , in each structure is then defined as

$$\Sigma = \int_{\varepsilon_V}^{\varepsilon_F} -COHP(E') E' dE'$$

where the COHP is also normalized by N_v .

Using these quantities, we produced the triangle plots shown in **Fig. 4a**. The ionicity, I , was defined as:

$$I_{A_\alpha B_\beta N_\gamma} = \frac{1}{\alpha + \beta + \gamma} \left(\alpha \frac{\delta_A}{s_A} + \beta \frac{\delta_B}{s_B} + \gamma \frac{\delta_N}{s_N} \right)$$

and quantifies the extent of electron transfer in the structure. The metallicity was defined as:

$$M_{A_\alpha B_\beta N_\gamma} = |\Sigma_{A-B} + \Sigma_{A-A} + \Sigma_{B-B}|$$

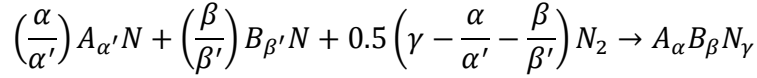
quantifying the net bonding energy of cation-cation interactions. The covalency, C , was defined as:

$$C_{A_\alpha B_\beta N_\gamma} = |\Sigma_{A-N} + \Sigma_{B-N} + \Sigma_{N-N}|$$

quantifying the net bonding energy for interactions containing nitrogen. To ensure each quantity (C , I , M) was of the same magnitude, each quantity was divided by the maximum of that quantity within the

dataset. In order to plot points on a triangle, the sum of each point, (C, I, M), must equal 1. Therefore, each quantity within each point was normalized by $C+I+M$.

To quantify the extent to which a given ternary was “N-rich” or “N-poor”, we compare the cation/anion ratios in the ternary to the ratios in the deep-hull binaries ($A_\alpha\text{-N}$, $B_\beta\text{-N}$) using the assumed formation reaction:



and subsequent condition for being rich or poor in nitrogen:

$$\gamma - \frac{\alpha}{\alpha'} - \frac{\beta}{\beta'} \geq 0 \rightarrow Nrich; \gamma - \frac{\alpha}{\alpha'} - \frac{\beta}{\beta'} < 0 \rightarrow Npoor.$$

This reaction was also used to compute the change in charge, $\Delta\delta$, across this formation reaction, as shown in **Fig. 4b**:

$$\Delta\delta_i = \delta_{i,A_\alpha B_\beta N_\gamma} - \frac{2}{\frac{\alpha}{\alpha'} + \frac{\beta}{\beta'} + \gamma} \left(\frac{\alpha}{\alpha'} \delta_{i,A_{\alpha'}N} + \frac{\beta}{\beta'} \delta_{i,B_{\beta'}N} + 0.5 \left(\gamma - \frac{\alpha}{\alpha'} - \frac{\beta}{\beta'} \right) \delta_{i,N_2} \right)$$

where δ_{i,N_2} was taken to be 0. A and B are defined as the least and most electronegative cations in the ternary.

Figure S.I.8.3 Scatterplot for change in ionicity of the more electronegative metal, B , and the nitrogen anion, N , with respect to the deepest-hull binaries, for stable Alkali-Metal-Nitride ternaries.

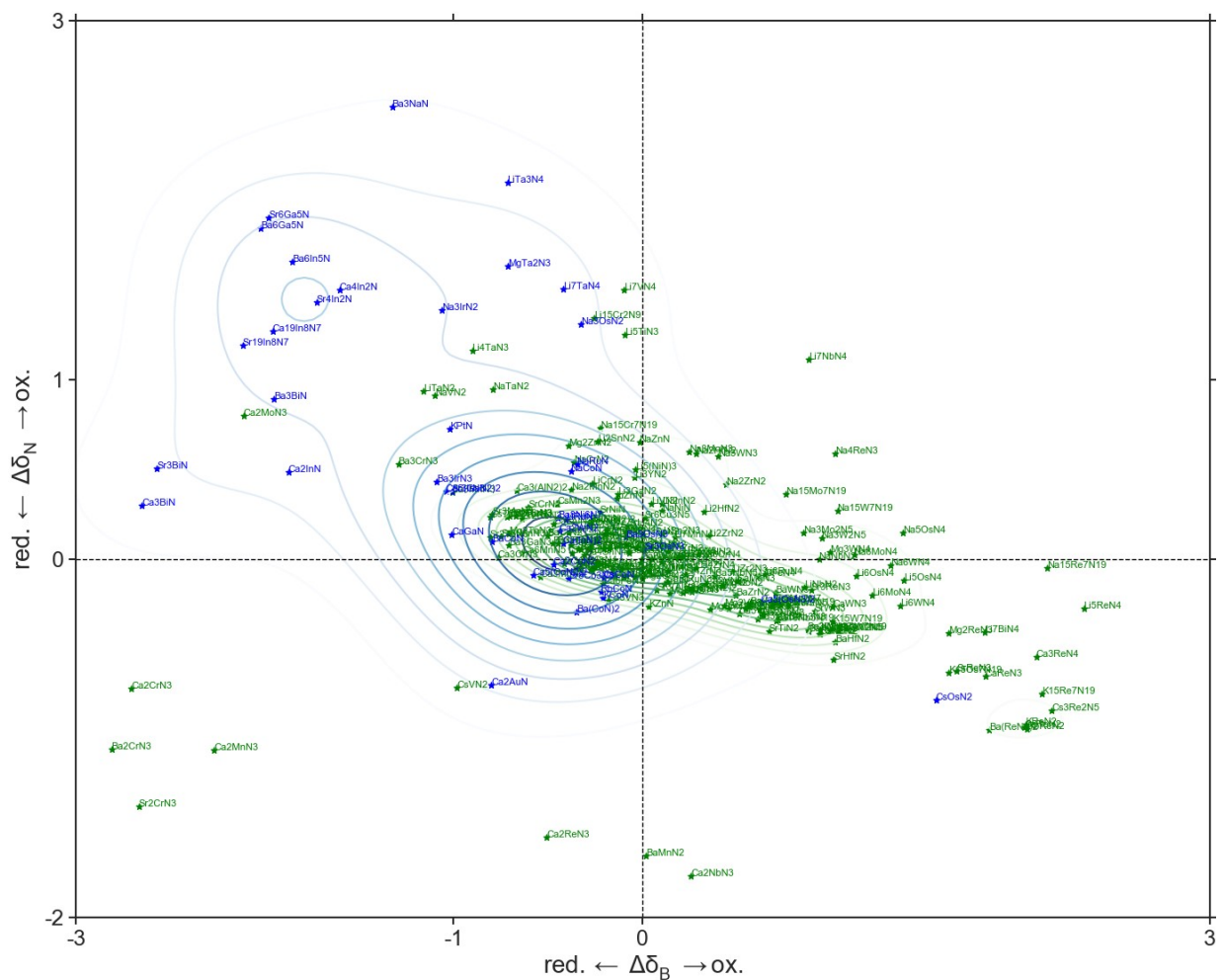
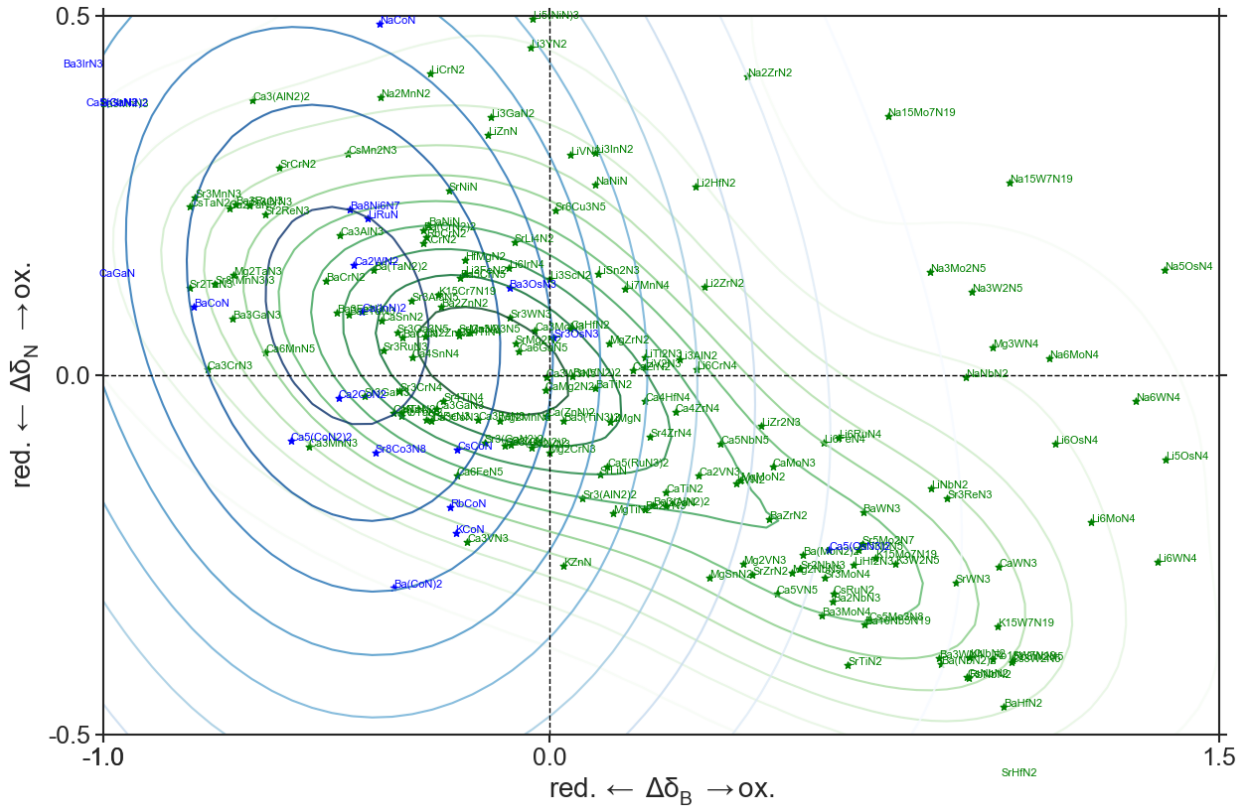
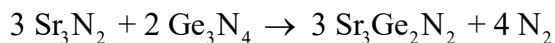
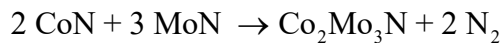


Figure S.I.8.4 Scatterplot for change in ionicity of the more electronegative metal, B , and the nitrogen anion, N , with respect to the deepest-hull binaries. Shown for stable Alkali-Metal-Nitride ternaries, magnified on the $-0.5 < \Delta\delta_N < 0.5$, and $-1.0 < \Delta\delta_B < 1.5$ ranges



S.I.9. Reductive Effect-stabilized structures

Formation of nitrogen-poor $\text{Co}_2\text{Mo}_3\text{N}$ and $\text{Sr}_3\text{Ge}_2\text{N}_2$ from the corresponding ‘deepest-hull’ binary nitrides proceeds by the following reactions:



In both systems, the metals are highly reduced compared to their corresponding binary nitrides, and there are strong metal-metal bonds in the ternary nitrides. As computed from the $\Delta\delta_{\text{N}}$ in **Figure 4b**, the electrons in these metal-metal bonds can be explained by oxidation of nitrogen (with respect to the corresponding binary nitrides).

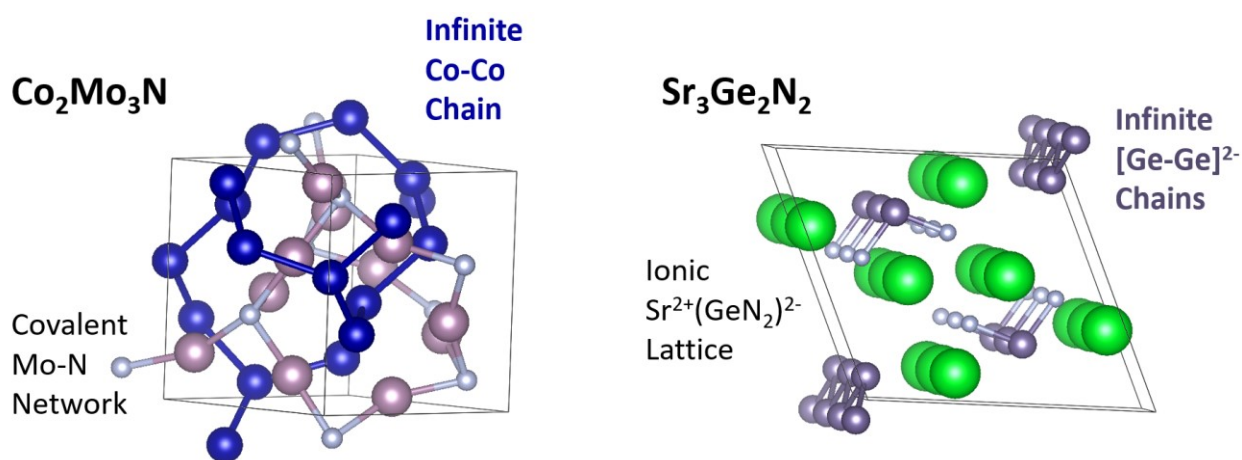


Figure S.I.9. Crystal structures of reductive effect stabilized $\text{Co}_2\text{Mo}_3\text{N}$ and $\text{Sr}_3\text{Ge}_2\text{N}_2$. $\text{Co}_2\text{Mo}_3\text{N}$ exhibits infinite 1-D chains of covalently-bonded $[\text{Co} - \text{Co}]_{\infty}$ intertwined within an extended Mo-N covalent network. $\text{Sr}_3\text{Ge}_2\text{N}_2$ features infinite 1-D $[\text{Ge} - \text{Ge}]_{\infty}^{2-}$ chains throughout an otherwise ionic $(\text{Sr}^{2+})_2[\text{GeN}_2]^{4-}$ lattice.

Supplemental Information References

- ¹ Gower, John C., and Pierre Legendre. "Metric and Euclidean properties of dissimilarity coefficients." *Journal of classification* 3.1 (1986): 5-48.
- ² Martin, Daniel P. "Clustering Mixed Data Types in R ." Clustering Mixed Data Types in R, *Wicked Good Data*, 22 June 2016, dpmartin42.github.io/posts/r/cluster-mixed-types.
- ³ Scerri, E. R. *Educ. Chem.* 2005, 42, 135–136. Scerri, E. R. *Hyle* 2005, 11, 127–145. Scerri, E. R. Relative Virtues of the Pyramidal and Left-Step Periodic Tables. In *The Periodic Table: Into the 21st Century*; Rouvray, D., King, B., Eds.; Science Research Press: Baldock, United Kingdom, 2004; pp 142–160
- ⁴ Dice, Lee R. "Measures of the amount of ecologic association between species." *Ecology* 26.3 (1945): 297-302.
- ⁵ Bar-Joseph, Ziv, David K. Gifford, and Tommi S. Jaakkola. "Fast optimal leaf ordering for hierarchical clustering." *Bioinformatics* 17.suppl_1 (2001): S22-S29.
- ⁶ Morgan, Dane, John Rodgers, and Gerbrand Ceder. "Automatic construction, implementation and assessment of Pettifor maps." *Journal of Physics: Condensed Matter* 15.25 (2003): 4361.
- ⁷ Sun, Wenhao, et al. "The thermodynamic scale of inorganic crystalline metastability." *Science Advances* 2.11 (2016): e1600225.
- ⁸ Sun, Wenhao, et al. "Thermodynamic Routes to Novel Metastable Nitrogen-Rich Nitrides." *Chemistry of Materials* 29.16 (2017): 6936-6946.
- ⁹ Bokeh Development Team (2018). Bokeh: Python library for interactive visualization, URL <http://www.bokeh.pydata.org>.
- ¹⁰ Arca, Elisabetta, et al. "Redox-Mediated Stabilization in Zinc Molybdenum Nitrides." *Journal of the American Chemical Society* 140.12 (2018): 4293-4301.
- ¹¹ Bauers, Sage R., et al. "Ternary Nitride Semiconductors in the Rocksalt Crystal Structure." *arXiv preprint arXiv:1810.05668*(2018).
- ¹² Toby, B. H., & Von Dreele, R. B. (2013). "GSAS-II: the genesis of a modern open-source all purpose crystallography software package". *Journal of Applied Crystallography*, 46(2), 544-549.
- ¹³ Schneider, Sebastian B., Rainer Frankovsky, and Wolfgang Schnick. "Synthesis of alkaline earth diazenides MAEN2 (MAE= Ca, Sr, Ba) by controlled thermal decomposition of azides under high pressure." *Inorganic chemistry* 51.4 (2012): 2366-2373.
- ¹⁴ Manz, Thomas A. "Introducing DDEC6 atomic population analysis: part 3. Comprehensive method to compute bond orders." *RSC Advances* 7.72 (2017): 45552-45581.
- ¹⁵ Manz, Thomas A., and Nidia Gabaldon Limas. "Introducing DDEC6 atomic population analysis: part 1. Charge partitioning theory and methodology." *RSC Advances* 6.53 (2016): 47771-47801.
- ¹⁶ Maintz, Stefan, et al. "LOBSTER: A tool to extract chemical bonding from plane-wave based DFT." *Journal of computational chemistry* 37.11 (2016): 1030-1035.